Validation of Aero-Load Estimator for Convair 880 Aircraft Flight Simulator Benchmark with Electro-Hydrostatic Actuators

Yamina BOUGHARI[1], Ruxandra Mihaela BOTEZ*,[1], Amir BANIAMERIAN[2], Ehsan SOBHANI TEHRANI[2], Armineh GARABEDIAN[2]

*Corresponding author
*,[1]ÉTS, Laboratory of Active Controls,
Avionics and AeroServoElasticity LARCASE,
1100 Notre Dame West, Montreal, Que., Canada, H3C-1K3,
Ruxandra.Botez@etsmtl.ca
[2]GLOBVISION,
780 Ste-Croix Ave., Suite 100, St. Laurent, Montreal, Que., Canada, H4L 3Y2

DOI: 10.13111/2066-8201.2021.13.3.2

Received: 18 June 2021/ Accepted: 12 August 2021/ Published: September 2021

Abstract: *Simulating an aircraft model using of high fidelity models of subsystems for its primary and secondary flight control actuators requires measuring or estimating aero-load data acting on flight control surfaces. One solution would be to incorporate the data recorded from flight tests, which is a time-consuming and costly process. This paper proposes another solution based on the validation of an aero-loads estimator or on the hinge moments predictor for fully electrical aircraft simulator benchmark. This estimator is based on an aerodynamic coefficient calculation methodology, inspired by Roskam's method that uses the geometrical data of the wing and control surfaces airfoils. The hinge moment values are found from two-dimensional lookup tables where the deflections of the control surfaces, aircraft altitude, and aircraft angles of attack are the input vectors of the tables; and the resulting hinge moment coefficients are the output vectors. The resulting hinge moment coefficients of the Convair 880 primary flight control surfaces are compared to those of its recorded flight test data; the results from the new software solution were found to be very accurate. Hinge moment lookup tables are integrated in the Convair 880 high fidelity flight simulation benchmark using mathematical models of energy-efficient Electro-Hydrostatic Actuators (EHA). Autopilot controls are designed for the roll, pitch, attitude and yaw damper motions using Proportional Integral (PI) controller scheduled for different flight conditions. Several different aircraft simulation scenarios are evaluated to demonstrate the efficacy and accuracy of the predicted hinge moment results.*

Key Words: *Aero-Load estimator, Hinge moment prediction, MEA, EHA, Aircraft simulation*

NOMENCLATURE

M_h: Hinge moment
$\bar{q}$: Dynamic pressure,
M: Mach number,
S: Total area of the flight control surface,
c: Airfoil chord
c_f: Control surface chord.

$C_{h,0}$: Zero control surface angle deflection hinge moment coefficient for surfaces with symmetrical airfoils;
$C_{h,\propto}$: Control surface hinge moment derivative due to the angle of attack.
$C_{h,\delta}$: Control surface hinge moment derivative due to the control surface deflection;
$C_{h,\delta t}$: Control surface hinge moment derivative due to the control surface tab deflection;
K_p: Proportional gain,
T_i: Integration time,
T_d: Derivation time.
δ: Flight control surface deflection
δ_t: Flight control surface tab deflection
$\propto_{eff}$: Effective angle of attack

1. INTRODUCTION

To promote greener aviation, which includes reducing greenhouse gas (GHG) emissions, aircraft designers have moved towards lighter and more reliable aircraft by producing More Electric Aircraft (MEA). For example, hydraulic systems require a significant amount of tubing along the aircraft fuselage and wings to ensure the pressure needed by actuation systems [1]. Furthermore, "redundancy" is required for primary control surfaces, which means that very bulky hydraulic tubing systems require protection against flammable liquids. In addition to the fuel consumption associated with these heavy systems, the maintenance time and cost of these aircrafts are notably high. Airbus was able to reduce the weight of the A380 aircraft by 1000 lb by changing the ailerons' hydraulic actuators to electro-hydrostatic actuators [2]-[4]. Furthermore, MEA systems are functioning very well using simple electrical structural solutions. In terms of safety, bulky hydraulic and mechanical systems can be replaced by electrical ones, saving weight and space as well as reducing maintenance requirements by eliminating the need for hydraulic tubing in aircraft. In addition, developing and installing MEA systems is less complex for airplane structures than using hydraulic technological systems, which need flammable fluid protection and heat shields; thus, expensive and lengthy certification requirements are reduced [3]. Any advantages to be gained from efficiency improvements in hydraulic systems are negligible due to their maturity compared to the improvements obtained by using electrical technology.

Electro-Hydrostatic Actuators (EHAs), known as Power by Wire PBW systems, are fully self-contained actuation systems. The power received from an electric source is transformed into the motion received from an input command signal [5]-[6]. The electrically powered systems gradually reduce the use of centralized systems for pneumatic and hydraulic power generation by using a small fixed-displacement pump driven by a speed-controlled electric motor. In addition to achieving power savings objectives, these PBW systems are composed of Line Replaceable Units (LRUs**)** [7], and thus they are easier to install or remove than conventional hydraulic actuators, drastically reducing maintenance costs. The EHA technology is the most reliable and suitable solution for "more-electric" aircraft, and is already being used in flight control systems on Lockheed Martin's F-35 Lightning II, and for the thrust vector control in the frame of the NASA's 2nd Generation Reusable Launch Vehicle program [6]. To design an aircraft flight control system, it is necessary to define the force that must be overcome to move a particular control surface at any given dynamic pressure and airspeed. This force acting from the hinge line of the control surface produces a moment, known as the "hinge moment" that varies with the angle of attack, the angle of control surface deflection, and the trim tab deflection.

However, defining the hinge moments for flight control surfaces in the early stages of aircraft control design is not an easy task. Furthermore, despite the aeronautical industry's need for an inexpensive and reliable method to estimate the control surfaces hinge moments, hinge moment prediction has not been a well defined area of research, unlike other aerodynamic coefficients estimation where new software have been developed [8]-[9]. In [10], a dynamic load simulator could reproduce the aerodynamic control surface hinge moments on the ground, but its procedure requires a set of real flight test data for different flight conditions that cover the whole flight envelope, including the magnitudes of control surfaces inputs for each flight condition.

Another related work is the AAA (Advanced Aircraft Analysis) software based on Roskam [11] that offers a preliminary aircraft design process from weight and performance sizing to aerodynamics, stability, and control analysis. Unlike the AAA software, this work presents a software solution for predicting only the hinge moment coefficients based on control surface geometrical data.

The proposed method is inspired by Roskam [11] and is based on Datcom that contains empirical relations derived from fitting curves to a large selection of experimental data. Predicted hinge moments are then interpolated via lookup tables with respect to the angle of attack α, sideslip angle β, and control surface deflection angles (elevators, ailerons, rudders) in the EHA dynamic surface block.

The EHA is also used in benchmark testing of a Convair 880 for all its primary flight control surfaces, utilized to simulate its behavior for different flight conditions using the roll, pitch and yaw attitude controls via Matlab/Simulink software.

The Convair 880 aircraft benchmark setup was used in the new fault identification and prognosis software that was designed in the project called "Diagnostic, Prognostic and Health Monitoring of Aircraft Flight Control System" led by GlobVision and partnered with Thales Avionics Canada (TCA).

This article is organized as follows: Section II offers a brief description of flight control surfaces, and Section III describes the hinge moment prediction procedure. Moreover, Section III presents a test case for the hinge moment estimation for Convair 880 flight control surfaces and a comparison of its results with real data recorded from flight tests.

Section IV describes a Simulink implementation of the hinge moment prediction in a 6-DOF aircraft flight dynamics model. Also, aircraft simulations were performed to show the efficacy and accuracy of this hinge moment prediction procedure for various flight conditions. Section IV concludes with a summary of these results. Finally, Section V concludes some recommendations for future work.

2. FLIGHT CONTROL SURFACES

Flight control surfaces are hinged surfaces situated on the aircraft wings as well as horizontal and vertical tails dedicated for controlling the aircraft's motion (pitch, yaw, roll) via manual or automatic control and driven by electro-hydraulic or electromechanical actuators.

As shown in Figure 1, a control surface model contains an EHA actuator model, an inner loop controller (typically a simple control gain), and a surface model. The surface model contains two blocks: one for the aerodynamic loads (i.e., the hinge moments) and the other for the control surface dynamics block.

The actuator models and the control surface dynamic models were provided by Thales Canada TCA and GlobVision. This paper presents a software solution developed for estimating the aerodynamics loads.

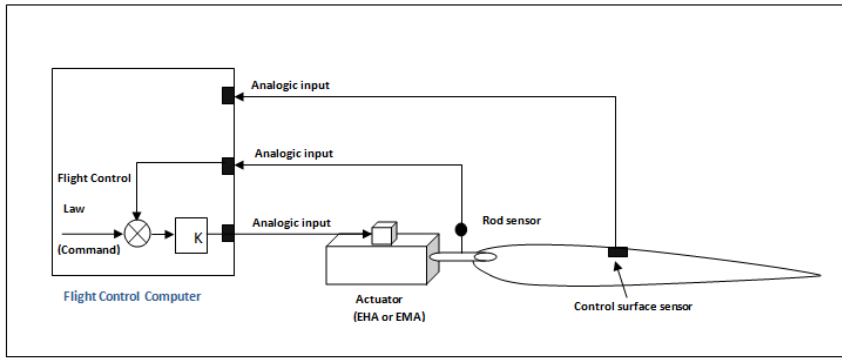

Figure 1. – Simplified block diagram of the actuator and control surface servo-loop

3. HINGE MOMENT PREDICTION

The hinge moment is the aerodynamic load or the force required to deflect a control surface, as shown in Figure 2. The hinge moment depends upon the aircraft attitude (deflection of control surface, angle of attack, etc.) and the flight conditions (Mach number and altitude), and therefore varies widely over the flight envelope.

For hinged control surfaces, the required actuation load can be characterized by the maximum hinge moment M_{hmax} obtained by the Federal Aviation Regulations FAR 25 for the commercial Convair 880 aircraft.

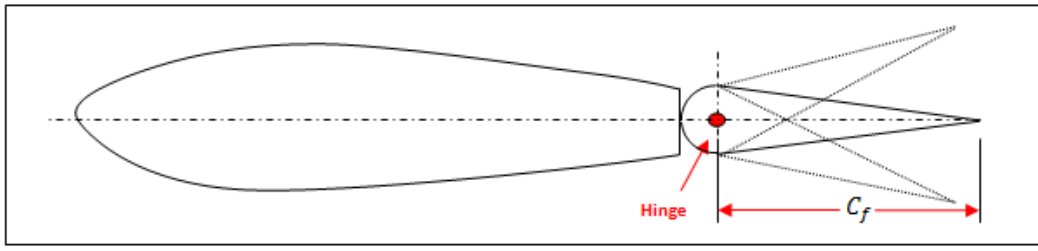

Figure 2. – Diagram of an airfoil with a control surface

The aerodynamic load or the hinge moment is usually provided by extensive flight tests, wind tunnel tests or CFD analysis, all of which are very time consuming and expensive.

An estimation of the aerodynamic loads can be used to predict hinge moments for primary control surfaces by a software programmed based on Roskam's equations and data presented in the form of curves.

The first step requires digitizing these data curves into an accessible digital dataset. Then, the digitized curves are approximated by a polynomial function.

Finally, the prediction algorithm uses mathematical equations and interpolation between the data curves to estimate the hinge coefficient. These equations and data curves are presented in the next sub-section.

3.1 Hinge Coefficient Estimation Algorithm

The hinge moments developed for primary control surfaces, such as ailerons, elevators, and rudder can be expressed in standard form using:

$$M_h = \bar{q} S \bar{c} C_{h\delta} \tag{1}$$

where

$$C_{h\delta} = C_{h,0} + C_{h,\alpha}(M)\alpha_{eff} + C_{h,\delta}(M,\delta)\delta + C_{h,\delta t}(M,\delta_t)\delta_t \quad (2)$$

where $\bar{q}$ is the dynamic pressure, S is the total surface of the flight control surface, $\bar{c}$ is the chord of the control surface, and $\propto_{eff}$. In addition,

$C_{h,\delta}$: is the control surface hinge moment derivative due to the control surface deflection;

$C_{h,0}$: is the zero control surface deflection and the zero tab angle deflection hinge moment coefficient for surfaces with symmetrical airfoils; and

$C_{h,\propto}$: is the control surface hinge moment derivative due to the angle of attack.

The 2D control surface's hinge moment derivative due to the angle of attack $\propto C_{h,\alpha}$ is estimated using the steps 1 to 4 as follows:

- **Step 1:**

Verify if the trailing-edge angle is satisfied:

$$\tan(\emptyset'_{te}/2) = \tan(\emptyset''_{te}/2) = \tan(\emptyset_{te}/2) = t/c \quad (3)$$

where $\emptyset'_{te}$ is the trailing edge angle defined as the angle between straight lines passing through points located at 90 % and 99% of the chord on the upper and lower airfoil surfaces;

$\emptyset''_{te}$ is the trailing edge angle defined as the angle between straight lines passing through points located at 95% and 99% of the chord on the upper and lower airfoil surfaces;

$\emptyset_{te}$ is the trailing edge angle defined as the angle between tangents to the upper and lower airfoil surfaces at the trailing edge.

These three trailing edge angles are shown in Figure 3.

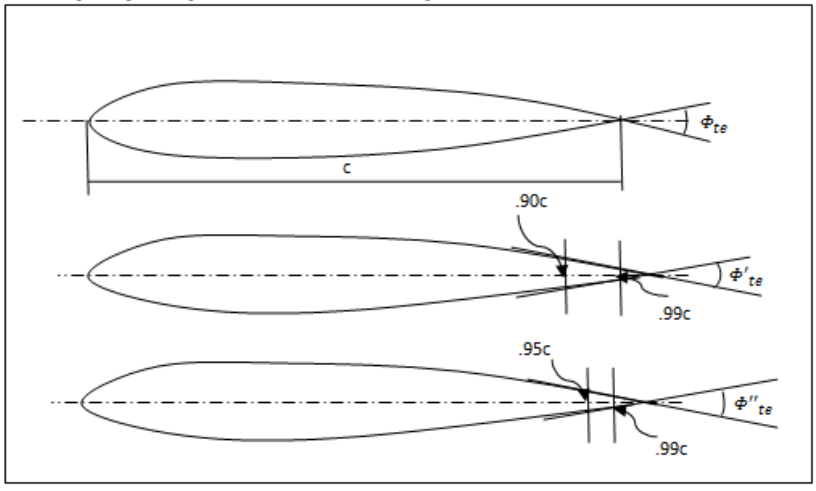

Figure 3. – Trailing edge angles

- **Step 2:**

Determine

$$C'_{h_\alpha} = \left\{C'_{h_\alpha}/C_{h_{\alpha_{theory}}}\right\} C_{h_{\alpha_{theory}}} \quad (4)$$

where $C'_{h_\alpha}/C_{h_{\alpha_{theory}}}$ is found from Figure 4 as function of flight control surface chord ratio c_f/c and based on different $C_{l_\alpha}/C_{l_{\alpha_{theory}}}$ shown in the legend in Figure 4. Figure 5 shows the value of $C_{l_\alpha}/C_{l_{\alpha_{theory}}}$ as a function of $\emptyset'_{te}$.

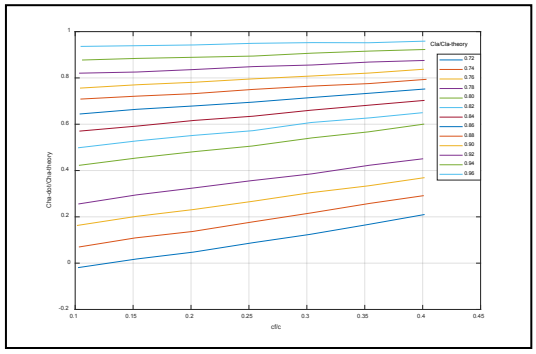

Figure 4. – $C'_{h_\alpha}/C_{h_{\alpha_{theory}}}$ versus cf/c for different $C_{L_\alpha}/C_{L_{\alpha_{theory}}}$

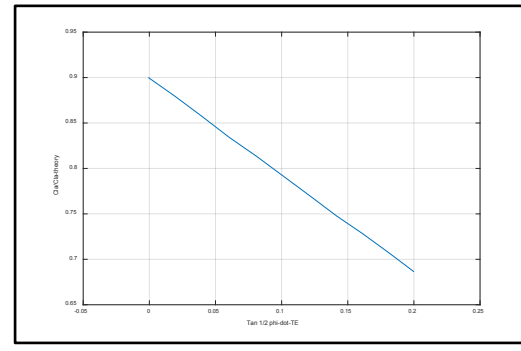

Figure 5. – $C_{l_\alpha}/C_{l_{\alpha_{theory}}}$ versus $\emptyset'_{te}$ for Reynolds number =10^6

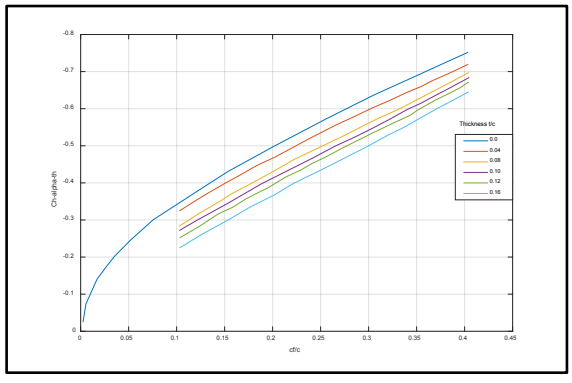

Figure 6. – $C_{h_{\alpha_{theory}}}$ versus the flight control surface chord ratio cf/c for several airfoil thickness t/c of a symmetrical airfoil

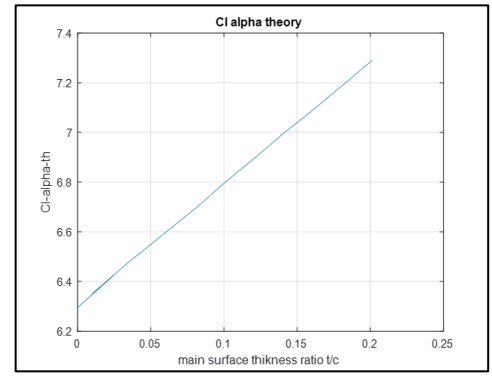

Figure 7. – $(C_{l_\alpha})_{theory}$ versus airfoil thickness t/c

➢ **Step 3:**

If the condition stated in equation (3) is satisfied, then:

$$C''_{h_\alpha} = C'_{h_\alpha} \tag{5}$$

If the condition presented in equation (3) is not satisfied, C''_{h_α} has to be computed from:

$$C''_{h_\alpha} = \left\{(C'_{h_\alpha}) + 2(C_{l_\alpha})_{theory}[1 - C_{l_\alpha}/(C_{l_\alpha})_{theory}\right\} * \{\tan\left(\frac{\emptyset''_{te}}{2}\right) - \left(\frac{t}{c}\right)\} \tag{6}$$

where (C'_{h_α}) is calculated using equation (4); and $\{C_{l_\alpha}/(C_{l_\alpha})_{theory}\}$ is obtained from Figure 5 as function of the trailing edge angle; $(C_{l_\alpha})_{theory}$ is obtained from Figure 7 at the corresponding thickness ratio $\left(\frac{t}{c}\right)$.

Corrections or adjustments will be made to account for different aircraft control surfaces nose shapes and for very good aerodynamic balance [11].

Note that the C'_{h_α} or C''_{h_α} value found from either Step 2 or Step 3 only apply to round nose control surfaces, which is the case considered in this paper. Therefore the balance expression $\frac{(C_{h_\delta})_{bal}}{C_{h_\delta}''}$ is equal to 1. If the control surface shape is not round then the balance expression will be determined from a curve presented in Roskam [11].

$$C_{h_\alpha} = \left\{ \{C'_{h_\alpha}/(C_{h_\alpha})_{theory}\}(C_{h_\alpha})_{theory} + 2(C_{l_\alpha})_{theory}\left[1 - \frac{C_{l_\alpha}}{(C_{l_\alpha})_{theory}}\right] * \left\{ tan\left(\frac{\emptyset''_{te}}{2}\right) - \left(\frac{t}{c}\right)\right\}\right\} \frac{(C_{h_\alpha})_{bal}}{C_{h_\alpha}''} * \frac{1}{\sqrt{1-M^2}} \tag{7}$$

➢ **Step 4**

The 2D hinge moment coefficient due to the surface control deflection $C'_{h,\delta}$ is computed by using equation (8), where $(C_{h_\delta})_{theory}$ is estimated by using Figure 8, and the value of $(C'_{h_\delta}/(C_{h_\delta})_{theory})$ is found from Figure 9.

$$C'_{h_\delta} = \{C'_{h_\delta}/(C_{h_\delta})_{theory}\}(C_{h_\delta})_{theory} \tag{8}$$

If the condition presented in equation (3) is not satisfied then C''_{h_δ} shall be computed from:

$$C''_{h_\delta} = 2(C_{l_\delta})_{theory}\left[1 - \frac{C_{l_\delta}}{(C_{l_\delta})_{theory}}\right] * \left\{ tan\left(\frac{\emptyset''_{te}}{2}\right) - \left(\frac{t}{c}\right)\right\} \tag{9}$$

where the value of $(C_{l_\delta})_{theory}$ and $\frac{C_{l_\delta}}{(C_{l_\delta})_{theory}}$ have to be found by using Figure 10, and Figure 11 respectively, and then the final value of the hinge coefficient due to the control surface deflection c_{h_δ} is calculated using:

$$c_{h_\delta} = \left\{ \{c'_{h_\delta}/(c_{h_\delta})_{theory}\}(c_{h_\delta})_{theory} + 2(c_{l_\delta})_{theory}\left[1 - \frac{c_{l_\delta}}{(c_{l_\delta})_{theory}}\right] * \left\{ tan\left(\frac{\emptyset''_{te}}{2}\right) - \left(\frac{t}{c}\right)\right\}\right\} \frac{(c_{h\delta})_{bal}}{c_{h_\delta}''} * \frac{1}{\sqrt{1-M^2}} \tag{10}$$

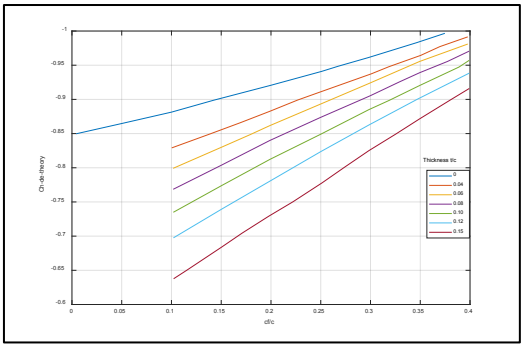

Figure 8. – $C_{h_{\delta_{theory}}}$ versus chord ratio cf/c for several Thicknesses t/c

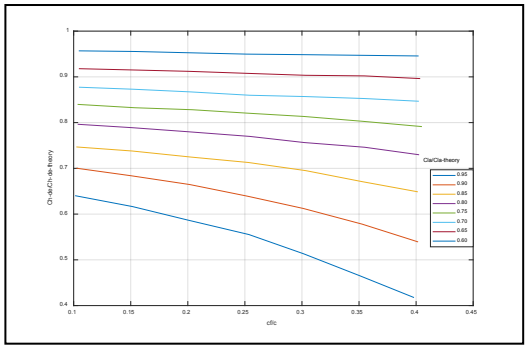

Figure 9. – $Ch'_\delta/Ch_{\delta_{theory}}$ versus cf/c for different values of $Cl_\alpha/Cl_{\alpha_{theory}}$

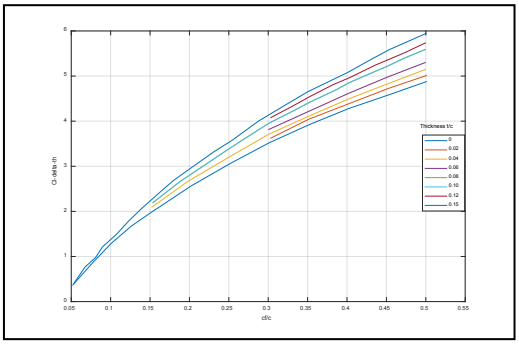

Figure 10. – $(C_{l_\delta})_{\text{theory}}$ versus cf/c for different thicknesses values t/c

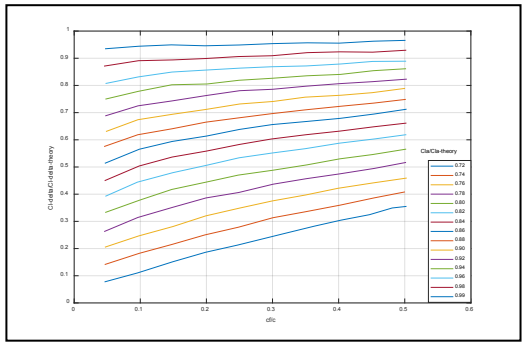

Figure 11. – $c_{l_\delta}/(c_{l_\delta})_{\text{theory}}$ versus cf/c for different $c_{l_\alpha}/(c_{l_\alpha})_{\text{theory}}$

We considered a round nose shape for the control surfaces of the Convair 880 aircraft, so the correction term of the balance expression $\frac{(C_{h\,\delta})_{bal}}{C_{h_\delta}''}$ is equal to 1.

The correction using the Mach effect expression $\frac{1}{\sqrt{1-M^2}}$ is integrated as a lookup table in the Simulink block of the hinge moment calculation. As in the case of Convair 880, the Mach effect from real flight test data is used instead.

The flow chart of the automated hinge moment estimation process/software is shown in Figure 12, including all the steps needed to determine the hinge coefficient for the primary control surfaces (elevator, rudder, and aileron) as previously described in this section.

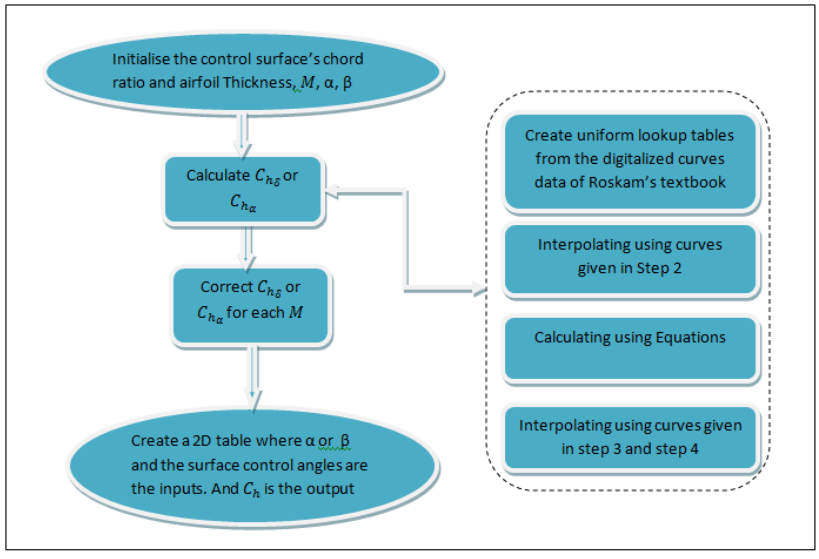

Figure 12. – Flow chart of the automated hinge moment estimation

4. TEST CASE

The hinge moment coefficients for the primary surfaces of the Convair 880 aircraft were estimated using the software outlined in Section III, and the estimates were compared with the hinge moment coefficients recorded from flight test data [12]-[14]. The Convair 880 geometrical data are listed in Table 1 [13] for its NACA 008-64 wing, with a span of 118.32

ft. The airfoils of the vertical and horizontal stabilizers were assumed to be those of the NACA-0012 airfoil, as suggested in [15].

Table 1. – Geometrical data of the Convair 880 wings and primary flight control surfaces

Convair 880 geometrical data	Elevator	Aileron	Rudder	Wing
Chord c (ft)	2.66	2.96	4.69	18.94
Surface S (ft^2)	88.28	2x27.37	82.44	2000
Inertia I (slug- ft^2)	33.60	2x19.11	54.56	-

Table 2 shows the hinge moment coefficients of the primary control surfaces for different flight conditions (FC) and Mach numbers (M) obtained from the Convair880 flight test data ([12], [14]).

Table 2. – Hinge moment coefficient obtained from fight tests of Convair 880

Flight Condition ========== Control Surface	FC1 M=0.2	FC2 M=0.24	FC3 M=0.6	FC4 M=0.7	FC5 M=0.8	FC6 M=0.86
Elevator	-0.326	-0.328	-0.336	-0.342	-0.31	-0.285
Tab Elevator	-0.287	-0.285	-0.297	-0.312	0.47	-0.352
Rudder	-0.214	-0.2125	-0.1626	-0.1345	-0.1491	-0.1924
Tab Rudder	-0.255	-0.253	-0.267	-0.27	-0.267	-0.265
Aileron	-0.607	-0.481	-0.236	-0.2233	-0.2005	-0.258
Tab Ailerons	-0.249	-0.227	-0.215	-0.226	-0.235	-0.213

4.1 Mach Effect

Using the flight test data [14] listed in Table 2, the Mach effect can be deduced by defining the reference flight test data as those corresponding to the smallest Mach number (M=0.2), and then dividing the hinge moment coefficient for each Mach number by the hinge moment coefficients of the reference flight condition. The Mach effects for the primary control surfaces are listed in Table 3 and plotted in Figures 13, 14 and 15 for elevator, rudder and aileron, respectively. As an example for the elevator, the Mach effect is calculated with:

$$M = 0.24 => M_{eff} = \frac{(Hm)_{0,24}}{(Hm)_{0.2}} = \frac{-0.328}{-0.326} \Leftrightarrow M_{eff} = 1.006 \quad (11)$$

Table 3. – Mach effect on primary flight control surfaces of the Convair 880

Mach	0.24	0.6	0.7	0.8	0.86
M_{eff}_Elevator	1.006	1.03	1.045	0.9509	0.8742
M_{eff}_Aileron	0.7924	0.3888	0.3679	0.3303	0.4250
M_{eff}_Rudder	0.9930	0.7598	0.6285	0.6967	0.5720

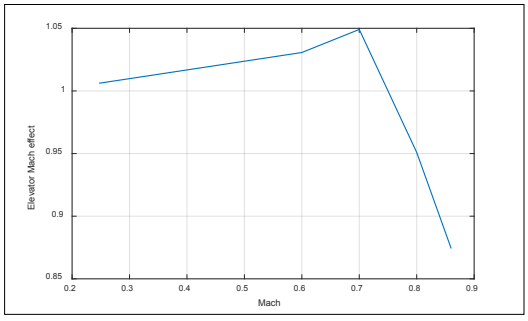

Figure 13. – Mach effect on the elevator

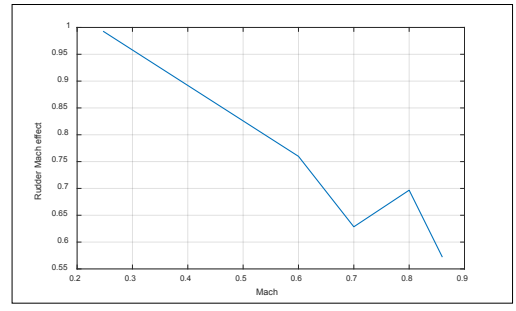

Figure 14. – Mach effect on the rudder

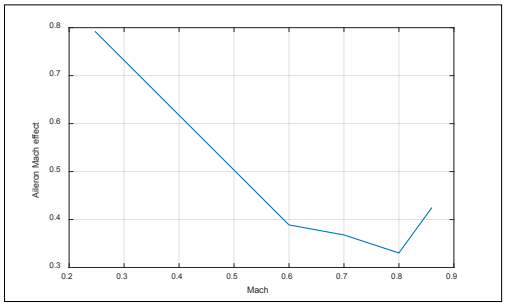

Figure 15. – Mach effect on the aileron

5. ANALYSIS OF RESULTS

The hinge coefficients estimated by the proposed algorithm were compared to those provided by real flight test data, and the results expressed in terms of relative errors are shown in Figures 16, 17 and 18 for all three primary control surfaces (elevator, rudder, and aileron) , as well as in Table 4. As shown in Table 4, from flight test data, the hinge moment coefficients derivatives with respect to angle of attack C_{h_α} are only available for the elevators. Where a relative error of 12.6% was obtained. The estimated hinge moment coefficients for control surface deflection derivative for the elevators C_{h_δ} were found to be much closer to those from the flight test data, thus representing a relative error of 7.5%. The estimated aileron hinge moment coefficients derivatives with the control surface deflection gave a relative error of 18.5% and the rudder hinge moment coefficients gave a relative error of 20% compared to their flight test data (Table 4). The accuracy of geometrical data assumed in the calculations and the presence of noise in flight tests may be important contributing factors explaining the relative errors found between the flight test data and the predicted results.

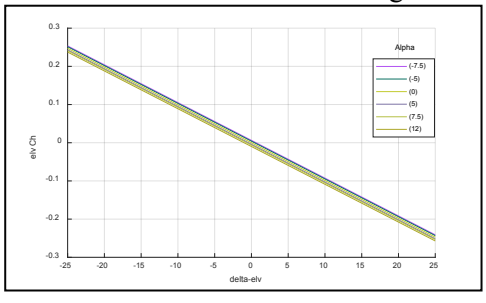

Figure 16. – Elevator hinge coefficient

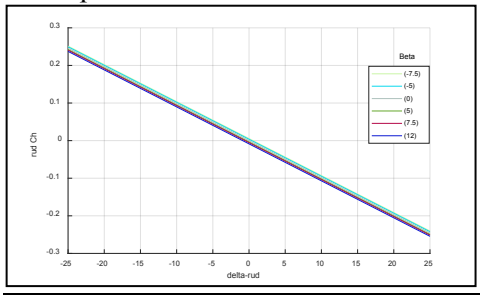

Figure 17. – Rudder hinge coefficient

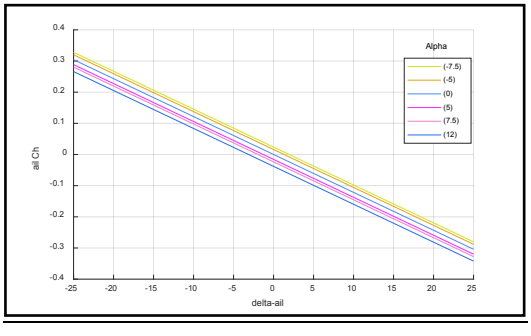

Figure 18. – Aileron hinge coefficient

Table 4. – The predicted hinge coefficients versus the Convair 880 flight test data

Hinge coefficient	Aileron	Elevator	Rudder
C''_{h_α} (predicted)	-0.18189	-0.0473	-0.0413
C_{h_α}(flight test)	-	-0.042	-
C''_{h_δ} (predicted)	-0.6969	-0.5667	-0.5635
C_{h_δ}(flight test)	-0.856	-0.613	-0.4667
Error between C''_{h_α} and C_{h_α} (%)	-	12.6%	-
Error between C''_{h_δ} and C_{h_δ} (%)	(18.5%)	(7.5%)	(20%)

6. SIMULINK IMPLEMENTATION AND RESULTS

6.1 Simulink Implementation of Hinge Moment

The hinge moment is converted into a linear force on the actuator, and is implemented in Simulink according to the equation (12), and multiplied by the "Mach effect". The Simulink block uses the Mach effect from flight test data as shown in Figure 19.

$$M_h = C_h . M_{eff} . q . S_{surf}\ \bar{c}_{surf} \tag{12}$$

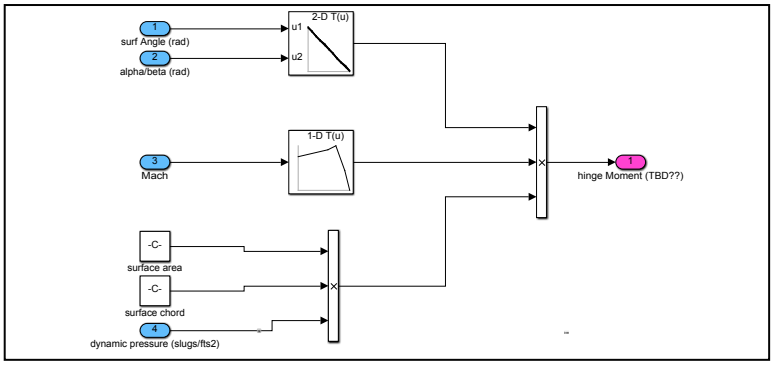

Figure 19. – Simulink Implementation of the Hinge Moment

6.2 6 DOFAircraft Model with Integrated Automatic Control

To demonstrate the efficiency of estimated hinge moments, simulations were performed on a Convair 880 civil aircraft model, highly representative of a nonlinear rigid-body aircraft model with a full set of flight control surfaces that were controlled by electro-hydraulic actuators. These aircraft surfaces were ailerons, spoilers, elevators, and a rudder.

The Convair 880 aircraft flight dynamics model was implemented in Matlab/Simulink using its 6-DOF equations of motion [16]-[19]. The aerodynamic coefficients for several flight conditions were provided from flight test data [14]. A large number of methodologies for a controller design and aircraft stability augmentation as well as flight quality standards [20] can be found in the literature. Proportional Integral Derivative (PID) control [21]-[24], LQR optimal control [25]-[27], and robust H-infinity control theories [28]-[33] are some of the control theories that were found to be very efficient in aircraft control as well as a many other industrial control applications.

The PID control theory was chosen in this paper for its ease of implementation. It was used to design autopilot for pitch attitude hold, roll attitude hold, heading and yaw damper, covering the whole flight envelope.

Many methods exist in the literature to tune the PID controller gains using trial-and-error process or using different optimization algorithms [21]-[24] to achieve minimum rise time, minimum overshoot, and/or minimum settling time.

The control error *e(t)* is the difference between the reference command *r(t)* and the measured output *y(t)*:

$$e(t) = r(t) - y(t) \tag{13}$$

The PID control law is given by equation (14):

$$u(t) = K_p \left[e(t) + \frac{1}{T_i} \int e(t')dt' + T_d \frac{1de(t)}{dt} \right] \tag{14}$$

In addition, different fault injection mechanisms for EHA faults such as hydraulic leakage across piston, null-bias fault in electro-hydraulic servo valve, servo valve gain degradation, etc. were integrated into the Simulink model by GlobVision team.

The aim of this was to test and validate the accuracy and robustness of the new fault detection, isolation and identification solutions developed by GlobVision with data from a near realistic simulation benchmark.

6.3 Simulations Results

The simulations were performed using the Rapid Accelerator mode of Simulink with the "ode 45" solver and fixed time step of 50 MHz. Different faults were injected during the simulations and their results are presented in this section.

Roll, pitch and yaw control tests performed for nominal, healthy (no fault) conditions provided very good reference tracking results.

Specifically, the aircraft followed the trajectories with a very small delay, without overshoot, and with a small steady state error as shown in Figure 20 for roll attitude control. Figure 21 shows the results of a roll control simulation performed by injecting a leakage fault for 1 second in the ailerons actuators.

Figures 22 and 23 show the errors obtained for two other types of faults/degradations injected in the ailerons actuators: (a) 80% decline in the nominal servo valve gain, the result of which is shown in Figure 22; and (b) 50% null-bias fault change due to 50% loss of stiffness in the retraction spring of the actuator, the result of which is shown on Figure 23. For all fault cases, the results are compared with those of nominal, healthy (no fault) simulations.

The healthy and those with different faults simulations show the efficacy of the hinge moment estimations, and its integration on the Convair 880 flight simulation benchmark.

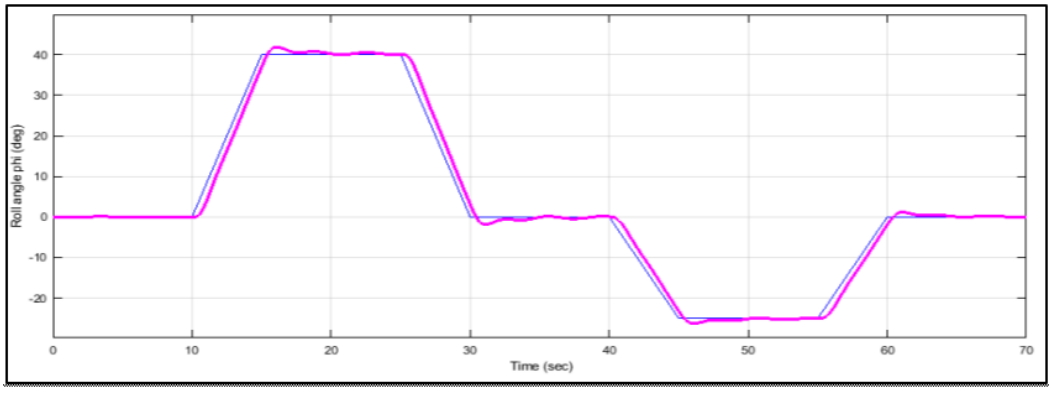

Figure 20. – Roll attitude control for healthy aircraft

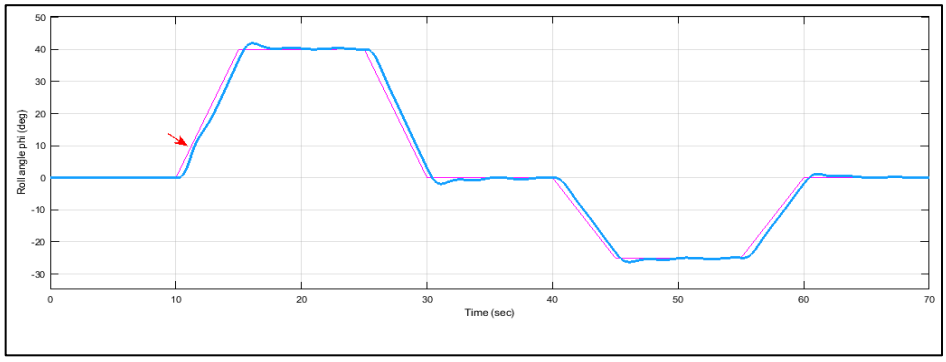

Figure 21. – Aircraft during roll response with fault of 0.0038 leakages for 1 sec on the left aileron actuator

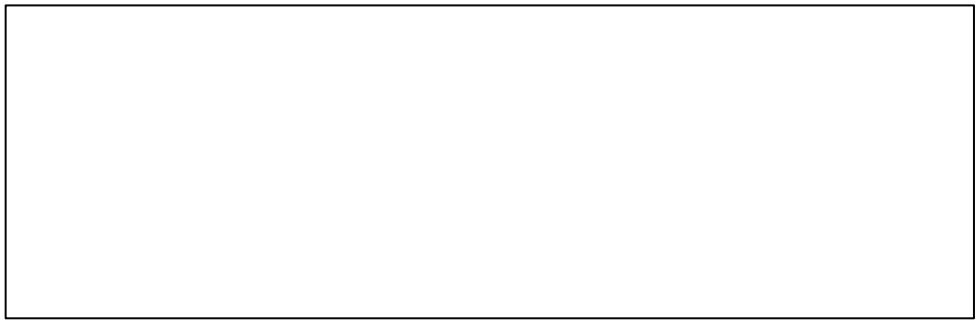

Figure 22. – Roll attitude control for aircraft with 80% of Kv error

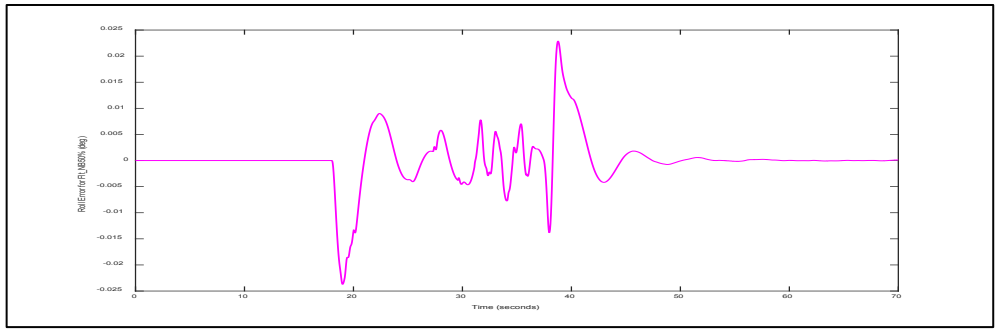

Figure 23. – Error between healthy and aircraft with fault of a 50 % null bias degradation during roll response

7. CONCLUSIONS AND RECOMMENDATIONS FOR FUTUR WORK

- High-fidelity HEA actuator models were integrated into a Convair 880 6-DOF aircraft flight dynamics model in which an autopilot system controlled pitch, roll, and heading attitudes to track different pre-defined, commanded trajectories using low-level control of flight control. The Convair 880 benchmark system was established to integrate various fault injection mechanisms to test and evaluate a novel model-based flight control diagnostic and health monitoring (DHM) solution. This work was developed under a CRIAQ (The Consortium for Research and Innovation in Aerospace in Quebec) project, which was realized as collaboration between partners from ÉTS, GlobVision, and Thales Avionics Canada.

- A software solution was developed to estimate the hinge moments acting as aerodynamic loads on flight control surfaces. Several tests of the software integrated into control surface models of the Convair 880 benchmark system showed that it provided quite accurate hinge moment estimates.
- The Convair 880 benchmark system showed that nonlinear simulation models can be used in the future to predict reconfigurable flight control system performance in the presence of degradations. This work also showed that it could be used in the design and analysis of new fault detection and identification algorithms.

ACKNOWLEDGMENTS

The work was financially supported by the MITACS and CRIAQ organizations. The authors would like to thank Mrs. Armineh Garabedian from GlobVision and Mr. Xavier Louis from Thales Avionics Canada for their support.

REFERENCES

[1] G. Qiao, G. Liu, Z. Shi, Y. Wang, S. Ma & T. C. Lim, A review of electromechanical actuators for More/All Electric aircraft systems, *Proceedings of the Institution of Mechanical Engineers, Part C: Journal of Mechanical Engineering Science*, **232**(22), 4128–4151, doi:10.1177/0954406217749869, 2018.

[2] * * * Advances in more-electric aircraft technologies, *Aircraft Engineering and Aerospace Technology*, vol. **73** no 3, https://doi.org/10.1108/aeat.2001.12773caf.002, 2001.

[3] S. Wang, *Motor-Control-More-Electric-Aircraft*, available, at http://mil-embedded.com/articles/motor-control-more-electric-aircraft/.

[4] D. Van Den Bossche, The A380 flight control electro-hydrostatic actuators, achievements and lessons learnt, *in ICAS 2006*, Hamburg, Germany, 2006.

[5] N. Alle, S. S. Hiremath, S. Makaram, K. Subramaniam & A. Talukdar, Review on electro hydrostatic actuator for flight control, *International Journal of Fluid Power*, **17**:2, 125-145, doi:10.1080/14399776.2016.1169743, 2016.

[6] * * * https://www.moog.com/products/actuators-servoactuators/actuation-technologies/electrohydrostatic.html.

[7] I. Chakraborty, D. N. Mavris, M. Emeneth, and A. Schneegans, A Methodology for Vehicle and Mission Level Comparison of More Electric Aircraft Subsystem Solutions: Application to the Flight Control Actuation System, *Proceedings of the Institution of Mechanical Engineers, Part G: Journal of Aerospace Engineering,* **229**, no. 6, 1088–1102, doi:10.1177/0954410014544303, 2015.

[8] N. Anton, R.M. Botez, and D. Popescu, New Methodologies for Aircraft Stability Derivatives Determination from Its Geometrical Data, In: *AIAA Atmospheric Flight Mechanics Conference*. p. 6046. American Institute of Aeronautics and Astronautics, Chicago, Illinois, 2009

[9] N. Anton, R. M. Botez, and D. Popescu, New methodology and code for Hawker 800XP aircraft stability derivatives calculations from geometrical data, *The Aeronautical Journal*, **114**(1156), 367-376, 2010.

[10] Y. Nam, S. K Hong, Force control system design for aerodynamic load simulator, *Control Engineering Practice,* vol. **10**, no 5, p. 549-558, doi :10.1016/S0967-0661(02)00004-7, 2002.

[11] Roskam, *Airplane Design, Part VI: Preliminary Calculation of Aerodynamic, Thrust and Power Characteristics*, Roskam Aviation and Engineering Corp. 550 p, 1988.

[12] L. V. Schmidt, *Introduction to aircraft flight dynamics*, American Institute of Aeronautics and Astronautics, 1998.

[13] J. S. Koziol, *Simulation Model for the Convair CV-880 and Boeing 720 B Aircraft-Autopilot Systems in the Approach Configuration*, No. DOT-TSC-FAA-71-12. United States. Federal Aviation Administration, 1971.

[14] R. K. Heffley and W. F. Jewell, *Aircraft handling qualities data*,1972.

[15] M. H. Sadraey, *Aircraft design: A systems engineering approach*, John Wiley & Sons, 2012.

[16] B. L. Stevens and F. L. Lewis, *Aircraft Control and Simulation*, Hoboken, N. J. John Wiley, 664 p, c2003.

[17] P. Goupil and G. Puyou, A High-Fidelity Airbus Benchmark for System Fault Detection and Isolation and Flight Control Law Clearance, *EUCASS Proceedings Series,* vol. **6**, p. 249-262, 2013.

[18] G. Ghazi, *Développement d'une Plateforme de Simulation et d'un Pilote Automatique- Application aux Cessna Citation X et Hawker 800XP*, Thesis, University of Quebec-École Polytechnique de Montréal, 212p, 2014.
[19] G. Ghazi and M. R. Botez, Development of a High-Fidelity Simulation Model for a Research Environment, In *SAE AeroTech Congress and Exhibition, AEROTECH 2015,* Seattle, WA, United States, September, 22-24*,* 2015*,* SAE Technical Papers, SAE International.
[20] * * * Standard, Military, 1990, *Flying Qualities of Piloted Aircraft. MIL-STD-1797A*, Department of Defense.
[21] T. L. Grigorie, R. M. Botez, A. V. Popov, M. Mamou and Y. Mebarki, A Hybrid Fuzzy Logic Proportionalintegral-Derivative and Conventional on-off Controller for Morphing Wing Actuation Using Shape Memory Alloy Part 1: Morphing System Mechanisms and Controller Architecture Design, *Aeronautical Journal*, vol. **116**, no 1179, p. 433-449, 2012a.
[22] T. L. Grigorie, A. V. Popov, R. M. Botez, M. Mamou and Y. Mebarki, On-off and Proportional-Integral Controller for a Morphing Wing. Part 1: Actuation Mechanism and Control Design 2, *Proceedings of the Institution of Mechanical Engineers, Part G: Journal of Aerospace Engineering*, vol. **226**, p. 131-145. 2012b.
[23] T. L. Grigorie, A. V. Popov, R. M. Botez, M. Mamou and Y. Mebarki, On-off and Proportional-Integral Controller for a Morphing Wing. Part 2: Control Validation - Numerical Simulations and Experimental Tests, *Proceedings of the Institution of Mechanical Engineers, Part G: Journal of Aerospace Engineering,* vol. **226**, p. 146-162, 2012c.
[24] T. L. Grigorie, R. M. Botez, A. V. Popov, M. Mamou and Y. Mébarki, A Hybrid Fuzzy Logic Proportional-Integral-Derivative and Conventional On-off Controller for Morphing Wing Actuation Using Shape Memory Alloy, Part 2: Controller Implementation and Validation, *The Aeronautical Journal*, vol. **116**, no 1179, p. 451-465, 2012d.
[25] Y. Boughari and R. M. Botez, Optimal Flight Control on the Hawker 800 XP Business Aircraft, *In IECON 2012 - 38th Annual Conference on IEEE Industrial Electronics Society*, October, 25-28, p. 5471-5476, 2012.
[26] Y. Boughari, G. Ghazi, and R. M. Botez, F. Theel, New Methodology for Optimal Flight Control Using Differential Evolution Algorithms Applied on the Cessna Citation X Business Aircraft - Part 1. Design and Optimization, *INCAS BULETTIN,* Bucharest, Vol. **9**, Iss. 2, pp. 31-44, https://doi.org/10.13111/2066-8201.2017.9.2.3, 2017.
[27] Y. Boughari, G. Ghazi, R. M. Botez, and F. Theel, New Methodology for Optimal Flight Control using Differential Evolution Algorithms applied on the Cessna Citation X Business Aircraft - Part 2. Validation on Aircraft Research Flight Level D Simulator, *INCAS BULETTIN,* Bucharest, Vol. **9**, Iss. 2, pp. 45-59, https://doi.org/10.13111/2066-8201.2017.9.2.4, 2017.
[28] Y. Boughari, G. Ghazi, F. Theel and R. M. Botez, Business Aircraft Flight Control System using Robust H-infinity Controllers on Cessna Citation X, *In Canadian Aeronautical Society Institute CASI AÉRO conference,* in Toronto, Ontario, Canada, on Mai 2nd, 2013.
[29] Y. Boughari, R. M.Botez, G. Ghazi and F. Theel, Evolutionary algorithms for robust cessna citation X flight control, *In SAE 2014 Aerospace Systems and Technology Conference, ASTC 2014*, Cincinnati, OH, United states September 23-25, 2014.
[30] Y. Boughari, R. M. Botez, G. Ghazi and F. Theel, Flight Control Clearance of the Cessna Citation X Using Evolutionary Algorithms, *Proceedings of the Institution of Mechanical Engineers, Part G: Journal of Aerospace Engineering*, p. 0954410016640821, 2016.
[31] Y. Boughari, R. M. Botez, F. Theel and G. Ghazi, Optimal Flight Control on Cessna X Aircraft Using Differential Evolution, *In IASTED International Conference on Modelling, Identification and Control, MIC 2014*, Innsbruck, Austria, February 17-19, p.189-198, 2014.
[32] Y. Boughari, G. Ghazi and M. R. Botez, Optimal Control New Methodologies Validation on the Research Aircraft Flight Simulator of the Cessna Citation X Business Aircraft, *In Science and Engineering for Reliable Energy Conference REMOO,* the 6th Conference and Workshop, in Budva, Montenegro on Mai 19th, 2016.
[33] Y. Boughari, G. Ghazi and M. R. Botez, Optimal Control New Methodologies Validation on the Research Aircraft Flight Simulator of the Cessna Citation X Business Aircraft, *In International Journal of Contemporary Energy*, Vol **3**, no 1, pp.9-18, Doi 10.14621/ce.20170102, 2017.